Available online at www.sciencedirect.com
ScienceDirect
Journal of Sound and Vibration 321 (2009) 305–318
JOURNAL OF SOUND AND VIBRATION
www.elsevier.com/locate/jsvi

Long transient phenomenon in nonlinear structural vibration

P. Frank Pai*

Department of Mechanical and Aerospace Engineering, University of Missouri, Columbia, MO 65211, USA

Received 24 August 2007; received in revised form 30 March 2008; accepted 18 September 2008
Handling Editor: S. Bolton
Available online 25 October 2008

Abstract

The long transient phenomenon in nonlinear structural vibrations is examined in detail by using a signal decomposition and processing method based on the empirical mode decomposition, Hilbert–Huang transform (HHT), and nonlinear dynamic characteristics derived from perturbation analysis. A sliding-window fitting (SWF) technique is derived to show the physical implication of Hilbert–Huang transform and other time–frequency decomposition methods. The SWF uses windowed regular harmonics and function orthogonality to simultaneously extract time-localized regular and/or distorted harmonics. Because of the use of pre-determined basis functions, function orthogonality, and windowed curve fitting for component extraction, it cannot extract accurate time-varying frequencies and amplitudes of harmonics distorted by nonlinearities. On the other hand, the HHT uses the apparent time scales revealed by the signal's local maxima and minima to sequentially sift distorted harmonics of different time scales, starting from high-frequency to low-frequency ones. Because Hilbert–Huang transform does not use predetermined basis functions and function orthogonality for component extraction, it provides more accurate signal decomposition and instant amplitudes and frequencies of extracted distorted harmonics. Numerical results show that the proposed HHT-based signal decomposition and processing method can accurately decompose nonlinear nonstationary signals and extract accurate intrawave amplitude and phase modulations, distorted harmonic response under a single-frequency harmonic excitation, and different types and orders of nonlinearities. Using this signal processing method, the long transient phenomenon in nonlinear vibrations is found to be caused by nonlinearities, coupling of transient and forced vibrations, and/or modal coupling of multiple modes.

1. Introduction

Dynamic characteristics of nonlinear systems are very different from those of linear systems in many ways and in both time and frequency domains. One well known phenomenon in nonlinear structural vibrations is the long transient time for developing a steady-state response, which is often attributed to a lack of significant damping [1]. This long transient phenomenon complicates nonlinear vibrations of flexible structures and it also significantly reduces the efficiency of nonlinear vibration absorbers based on 2:1 or other higher-order internal resonances [2–4].

*Tel.: +1 573 884 1474; fax: +1 573 884 5090.
E-mail address: paip@missouri.edu

0022-460X/$ - see front matter © 2008 Elsevier Ltd. All rights reserved.
doi:10.1016/j.jsv.2008.09.034

The exact forced response of a harmonically excited linear mass–damper–spring (m–c–k) system is given as [5]

$$m\ddot{u} + c\dot{u} + ku = m(\ddot{u} + 2\zeta\omega\dot{u} + \omega^2 u) = F_0 \cos \Omega t,$$
$$u(t) = ae^{-\zeta\omega t} \cos(\omega_d t - \theta) + A_0 \cos(\Omega t - \phi), \tag{1a}$$

$$A_0 = F_0|H(\Omega)| = \frac{F_0}{k\sqrt{(1-\Omega^2/\omega^2)^2 + (2\Omega\zeta/\omega)^2}}, \quad \phi = \tan^{-1}\frac{2\Omega\zeta/\omega}{1-\Omega^2/\omega^2},$$
$$H(\Omega) = \frac{1}{k - m\Omega^2 + j\Omega c} = \frac{1}{k(1-\Omega^2/\omega^2 + j2\Omega\zeta/\omega)} = |H(\Omega)|e^{-j\phi}, \tag{1b}$$

$$a = \sqrt{\omega_d^2(u_0 - A_0\cos\phi)^2 + [v_0 + \zeta\omega(u_0 - A_0\cos\phi) - \Omega A_0 \sin\phi]^2}/\omega_d,$$
$$\theta = \tan^{-1}\frac{v_0 + \zeta\omega(u_0 - A_0\cos\phi) - \Omega A_0 \sin\phi}{(u_0 - A_0\cos\phi)\omega_d}, \quad \omega_d \equiv \omega\sqrt{1-\zeta^2}, \tag{1c}$$

where $\dot{u} \equiv du/dt$, and u_0 and v_0 are initial displacement and velocity, respectively. Eqs. (1a) and (1c) show that, although the transient vibration amplitude a and phase θ are affected by the excitation frequency Ω and amplitude F_0 (through A_0), the transient part vibrates at the damped natural frequency ω_d. Eqs. (1a) and (1b) show that the steady-state part is not affected by initial conditions and it vibrates at the excitation frequency Ω with a constant amplitude A_0 at any time. If $\Omega = \omega$, it follows from Eq. (1b) that $F_0 = 2\zeta k A_0 = c\omega A_0 = c\Omega A_0$, $\phi = \pi/2$, $\dot{u} = \Omega A_0 \cos \Omega t$, and hence $F_0 \cos \Omega t = c\dot{u}$ after the transient part dies out. In other words, the excitation force is balanced out by the damping force, and the system vibrates like a free undamped oscillator.

To show nonlinear dynamic characteristics we consider the following harmonically excited weakly nonlinear second-order oscillator and its second-order perturbation solution [1,6]:

$$m\ddot{u} + c\dot{u} + ku + m\alpha u^3 = F_0 \cos \Omega t, \tag{2a}$$

$$u(t) = u_h(t) + a\cos(\Omega t - \phi) + a_3 \cos(3\Omega t - 3\phi) + \cdots, \quad a_3 = \frac{\alpha a^3}{32\Omega^2} \ll a,$$
$$= u_h(t) + \hat{a}(t)\cos(\Omega t - \phi + \Theta(t)) + \cdots, \tag{2b}$$

$$\hat{a}(t) \equiv \sqrt{a^2 + a_3^2 + 2aa_3\cos(2\Omega t - 2\phi)} \approx a + a_3\cos(2\Omega t - 2\phi),$$
$$\Theta(t) \equiv \tan^{-1}\frac{a_3\sin(2\Omega t - 2\phi)}{a + a_3\cos(2\Omega t - 2\phi)} \approx \frac{a_3}{a}\sin(2\Omega t - 2\phi),$$
$$\hat{\Omega}(t) = \Omega + \dot{\Theta} \approx \Omega + \frac{2\Omega a_3}{a}\cos(2\Omega t - 2\phi), \tag{2c}$$

$$\left(\frac{3\alpha}{8\omega}\right)^2 a^6 - \frac{3\alpha\sigma}{4\omega}a^4 + (\sigma^2 + \zeta^2\omega^2)a^2 - \left(\frac{F_0}{2\omega m}\right)^2 = 0, \quad \sigma \equiv \Omega - \omega, \ \ \omega \equiv \sqrt{\frac{k}{m}}, \tag{2d}$$

$$\phi = \tan^{-1}\frac{\zeta\omega}{3\alpha a^2/(8\omega) - \sigma}. \tag{2e}$$

Eq. (2d) shows that the amplitude a may have three possible solutions and each has its own domain of attraction on the phase plan $u - \dot{u}$. Hence, the obtained steady-state solution depends on initial conditions. If the excitation force is balanced out by the damping force (i.e., $F_0 = 2\omega^2 m\zeta a = c\omega a$ in Eq. (2d)), it follows from Eq. (2d) that $a^2 = 8\omega\sigma/3\alpha$, which is the so-called *backbone* equation representing the relation between the free undamped vibration frequency (i.e., natural frequency $\hat{\omega} \equiv \omega + \sigma = \omega + 3\alpha a^2/8\omega$) with the vibration amplitude a. Eq. (2c) shows that the steady-state part is a distorted harmonic having time-varying frequency and amplitude modulating at a frequency 2Ω. On the other hand, Eq. (2b) shows that the steady-state part consists of two regular harmonics and hence its spectrum has two spectral lines at Ω and 3Ω. For a nonlinear

single-degree-of-freedom system, the extra spectral line can be used to identify the nonlinearity. However, for a nonlinear continuous or multiple-degree-of-freedom system with internal resonance, it is difficult to identify nonlinearities from response spectra because each directly or indirectly excited mode has a distorted harmonic motion and the extra spectral lines from all involved modes are difficult to be separated and recognized.

The complete solution shown in Eq. (2b) is assumed to consist of a transient part and a part that is steady at any time, just like the linear case shown in Eq. (1a). Because of nonlinearity, the complete solution can only be obtained by direct numerical integration, and the transient part $u_h(t)$ is usually not examined because it is difficult to extract it from a nonstationary signal. In this paper we present a method for extracting the transient part and show that the transient part has an expected amplitude-dependent vibration frequency and it also delays the development of the steady-state part, which invalidates the form assumed in Eq. (2b) and is a nonlinear phenomenon never investigated in the literature before. The proposed signal processing method is based on Hilbert–Huang transform (HHT).

Because the operation time for any movement of a dynamical system is always limited, transient response often exists, especially in systems with control actions, high operational speeds, and/or high flexibility. Hence, methods for dynamics characterization and system identification need to deal with transient responses, and the proposed method is valid for many applications in signal processing and system identification of linear and nonlinear systems.

2. Signal decomposition method

HHT is a new technique developed after short-time Fourier transform and wavelet transform for time–frequency decomposition of linear/nonlinear stationary/nonstationary signals, and it is essentially different from Fourier and wavelet transforms because HHT does not use pre-determined basis functions and the orthogonality between the basis functions and the signal itself to extract components [7–12]. However, HHT is not good at decomposing a signal consisting of two similar harmonics. To help with these situations and to reveal the mathematical implications and characteristics of HHT we first derive a sliding-window fitting (SWF) method using a set of pre-determined regular harmonics for extracting local distorted harmonics.

2.1. Sliding-window fitting

If a time signal $u(t)$ is identified from its Fourier spectrum to have two major frequencies ω_1 and ω_2 ($<\omega_1$), one can assume that

$$\begin{aligned} u(t) &= \sum_{k=1}^{2}[e_k\cos(\omega_k t)+\hat{e}_k\sin(\omega_k t)]+e_3+\hat{e}_3 t+e_4 t^2 \\ &= \sum_{k=1}^{2}[C_k\cos(\omega_k \bar{t})+\hat{C}_k\sin(\omega_k \bar{t})]+C_3+\hat{C}_3\bar{t}+C_4\bar{t}^2, \end{aligned} \tag{3}$$

where e_k and $\hat{e}_k$ are constants, $\bar{t}\,(\equiv t-t_s)$ is a shifted time, t_s is the observed time instant, and

$$\begin{aligned} &C_k=\sqrt{e_k^2+\hat{e}_k^2}\cos(\omega_k t_s-\phi_k),\quad \hat{C}_k=-\sqrt{e_k^2+\hat{e}_k^2}\sin(\omega_k t_s-\phi_k),\quad \phi_k=\tan^{-1}\hat{e}_k/e_k, \\ &C_3=e_3+\hat{e}_3 t_s+e_4 t_s^2,\quad \hat{C}_3=\hat{e}_3+2e_4 t_s,\quad C_4=e_4. \end{aligned} \tag{4}$$

To obtain the coefficients C_k and $\hat{C}_k$ for the data point at $\bar{t}=0$ we use data points around $t=t_s$ to minimize the square error E_{rror} defined as

$$E_{\text{rror}}\equiv\sum_{i=-m}^{m}\alpha^{|i|}(u_i-\hat{u}_i)^2, \tag{5}$$

where u_i represents $u(\bar{t}_i)$ from Eq. (3) and $\hat{u}_i$ represents the experimental data at $\bar{t}_i$. The total number of points used is $2m+1$, $\alpha^{|i|}$ is the weighting factor, and the forgetting factor $\alpha\,(\leqslant 1)$ is chosen by the user. The seven

equations to determine C_i and $\hat{C}_i$ for the point at $\bar{t}=0$ are given by

$$\frac{\partial E_{\text{rror}}}{\partial C_j}=\sum_{i=-m}^{m}2\alpha^{|i|}(u_i-\hat{u}_i)\frac{\partial u_i}{\partial C_j}=0, \tag{6}$$

where C_j, $j=1,\ldots,7$, represent $C_1,\hat{C}_1,C_2,\hat{C}_2,C_3,\hat{C}_3$, and C_4. Because, for example, $\partial u_i/\partial C_1=\cos(\omega_1\bar{t}_i)$, Eq. (6) shows that C_j are extracted by using the orthogonality between the predetermined functions used in Eq. (3) and the experimental data $\hat{u}_i$. After C_j and $\hat{C}_j$ are determined, it follows from Eq. (3) that

$$u(t_s)=C_1+C_2+C_3,\quad \dot{u}(t_s)=\omega_1\hat{C}_1+\omega_2\hat{C}_2+\hat{C}_3,\quad \ddot{u}(t_s)=-\omega_1^2C_1-\omega_2^2C_2+2C_4. \tag{7}$$

It indicates that $u(t_s)$ consists of the instantaneous value C_1 of the harmonic $\cos\omega_1\bar{t}$, the instantaneous value C_2 of the harmonic $\cos\omega_2\bar{t}$, and the low-frequency moving average C_3. More importantly, each of u, $\dot{u}$, and $\ddot{u}$ is decomposed into three components of different frequencies. Furthermore, it follows from Eq. (4) that

$$A_k\equiv\sqrt{C_k^2+\hat{C}_k^2}=\sqrt{e_k^2+\hat{e}_k^2},\quad \theta_k\equiv\tan^{-1}\frac{-\hat{C}_k}{C_k}=\omega_k t_s-\phi_k, \tag{8}$$

where A_1 and A_2 are the instantaneous amplitudes of the first and second harmonics, respectively. To reduce the influence of noise on the calculated instantaneous frequency ω_i, each ω_i at $t=t_s$ can be computed by averaging over $2p\Delta t$ (e.g., $p=2$) as

$$\omega_k\equiv\frac{\mathrm{d}\theta_k}{\mathrm{d}t}\approx\frac{\sum_{i=-p+1}^{p}[\theta_k(t_s+\mathrm{i}\Delta t)-\theta_k(t_s+(\mathrm{i}-1)\Delta t)]}{2p\Delta t}. \tag{9}$$

This method can be used to extract as many harmonics as needed by adding to Eq. (3) major harmonics identified from the signal's Fourier spectrum. Because harmonic functions are not orthogonal to the polynomial $C_3+\hat{C}_3\bar{t}+C_4\bar{t}^2$, one needs to choose an appropriate window length to enforce the orthogonality in order to obtain unique values for each C_j. Numerical results show that an appropriate choice is $2p\Delta t\geqslant 4\pi/\omega_2$, i.e., two periods of the lowest-frequency harmonic.

Unfortunately, the summation over the localized time interval $-m\Delta t\leqslant\bar{t}\leqslant m\Delta t$ in Eq. (6) locally averages the result. Hence, the obtained amplitudes and frequencies are not really instantaneous values. Furthermore, the ω_1 and ω_2 in Eq. (3) need to be known in order to accurately decompose the $u(t)$ into three components of different frequencies. If the ω_i are not known and many different values are used in Eq. (3), the signal will be decomposed into many components, which is the essence of windowed Fourier transform [13]. In other words, the use of pre-determined basis functions (see Eq. (3)) and the orthogonality between the basis functions and the signal to be decomposed causes the inaccuracy of the extracted amplitudes and frequencies.

2.2. Hilbert–Huang transform

HHT is essentially different from short-time Fourier transform and wavelet transform because it does not use pre-determined basis functions (i.e., regular harmonics or wavelets) and the orthogonality between the basis functions and the signal itself to extract components. The first step of HHT is to use the empirical mode decomposition (EMD) method to sequentially decompose a time series $u(t)$ into n intrinsic mode functions (IMFs) $c_i(t)$ and a residual r_n as [7,8]

$$u(t)=\sum_{i=1}^{n}c_i(t)+r_n(t), \tag{10}$$

where c_1 has the shortest characteristic time scale and is the first extracted IMF. The characteristic time scale of c_1 is defined by the time lapse between the extrema of u. Once the extrema are identified, compute the upper envelope by connecting all the local maxima using a natural cubic spline, compute the lower envelope by connecting all the local minima using another natural cubic spline, subtract the mean of the upper and lower envelopes, m_{11}, from the signal, and then treat the residuary signal as a new signal. Repeat these steps for K times until the left signal has a pair of symmetric envelopes (i.e., $m_{1K}\approx 0$), and then define c_1 as

$$c_1\equiv u-m_{11}\cdots-m_{1K}. \tag{11}$$

This sifting process eliminates low-frequency riding waves, makes the wave profile symmetric, and separates the highest-frequency IMF from the current residuary signal. During the sifting process for each IMF a deviation D_v is computed from the two consecutive sifting results as

$$D_v \equiv \sqrt{\frac{\sum_{i=1}^{N}[c_{1k}(t_i)-c_{1k-1}(t_i)]^2}{\sum_{i=1}^{N}c_{1k-1}^2(t_i)}}, \tag{12}$$

where, for example, $c_{1k} \equiv u - m_{11} \cdots - m_{1k}$, $t_i = \mathrm{i}\Delta t$, and $T(= N\Delta t)$ is the sampled period. A systematic method to end the iteration is to limit D_v to be a small number and/or to limit the maximum number of iterations. After c_1 is obtained, define the residual r_1, treat r_1 as the new data, and repeat the steps shown in Eq. (11) to obtain other c_i $(i = 2, \ldots, n)$ as

$$c_n = r_{n-1} - m_{n1} \cdots - m_{nK}, \quad r_{n-1} \equiv u(t) - c_1 \cdots - c_{n-1}. \tag{13}$$

The whole sifting process can be stopped when the residual $r_n(= r_{n-1} - c_n)$ becomes a monotonic function from which no more IMF can be extracted. In other words, the last IMF has no more than two extrema. For data with a trend, r_n should be the trend.

The second step of HHT is to perform Hilbert transform and compute the time-dependent frequency ω_i and amplitude A_i of each c_i. After all $c_i(t)$ are extracted, one can perform Hilbert transform to obtain $d_i(t)$ from each $c_i(t)$. Then one can combine the $c_i(t)$ and $d_i(t)$ into a complex function $z_i(t)$ and use Eq. (10) with r_n being neglected to obtain

$$\begin{aligned} &z_i(t) \equiv c_i(t) + jd_i(t) = A_i \mathrm{e}^{j\theta_i}, \quad A_i \equiv \sqrt{c_i^2 + d_i^2}, \quad \theta_i \equiv \tan^{-1} d_i/c_i, \\ &u(t) = \mathrm{Real}\left(\sum_{i=1}^{n}[c_i(t) + jd_i(t)]\right) = \mathrm{Real}\left(\sum_{i=1}^{n} A_i(t)\mathrm{e}^{j\theta_i(t)}\right). \end{aligned} \tag{14}$$

Eq. (14) reveals that HHT is a time-varying signal decomposition method and each IMF has a time-varying amplitude A_i and a time-varying frequency ω_i $(\equiv \mathrm{d}\theta_i/\mathrm{d}t)$. To reduce the influence of noise on the calculated frequencies, each ω_i can be obtained by averaging over $2p\Delta t$, as shown in Eq. (9). However, for damage detection applications, it is better to compute the true instantaneous ω_i and other time derivatives using

$$\begin{aligned} &\dot{A}_i = \frac{c_i\dot{c}_i + d_i\dot{d}_i}{A_i}, \quad \ddot{A}_i = \frac{\dot{c}_i^2 + c_i\ddot{c}_i + \dot{d}_i^2 + d_i\ddot{d}_i - \dot{A}_i^2}{A_i}, \\ &\omega_i = \frac{\mathrm{d}\theta_i}{\mathrm{d}t} = \frac{c_i\dot{d}_i - \dot{c}_i d_i}{A_i^2}, \quad \dot{\omega}_i = \frac{c_i\ddot{d}_i - \ddot{c}_i d_i - 2\omega_i(c_i\dot{c}_i + d_i\dot{d}_i)}{A_i^2}, \end{aligned} \tag{15}$$

which are derived from Eq. (14). The $\dot{c}_i$, $\dot{d}_i$, $\ddot{c}_i$, and $\ddot{d}_i$ needed in Eq. (15) can be computed using the inverse Fourier transform and multiplication in the frequency domain without numerical differentiation in the time domain. Because distorted harmonics with time-varying frequencies and amplitudes are allowed in the data decomposition, HHT does not need spurious harmonics to represent nonlinear/nonstationary signals. As shown in Eq. (10), the c_i represent a complete set of basis functions and they are local and adaptive, but they might not be orthogonal to each other. However, even regular harmonics of different frequencies are not exactly orthogonal, and the EMD does not use orthogonality of functions to extract c_i, which makes HHT essentially different from Fourier and wavelet transforms [14,15]. Theoretically speaking, signal decomposition by wavelet transform can be performed without using pre-determined basis functions and function orthogonality if signal dependent wavelet filter banks can be systematically computed [15]. However, it is still an open problem for researchers.

3. Numerical results

To show the long transient phenomenon in nonlinear structural vibrations we consider nonlinear systems of one and two degrees of freedom.

3.1. Single-degree-of-freedom system

We consider the following nonlinear oscillator:

$$m\ddot{u} + c\dot{u} + ku + k\alpha u^3 = m(\ddot{u} + 2\zeta\omega\dot{u} + \omega^2 u + \omega^2\alpha u^3) = F_0 \sin \Omega t, \tag{16a}$$

$$\Leftrightarrow \ddot{u} + 2\zeta\omega\dot{u} + \omega^2(u + \alpha u^3) = F \sin \Omega t, \quad F \equiv F_0/m. \tag{16b}$$

If the time t is normalized into a nondimensional time τ using the linear vibration period $2\pi/\omega$ and the displacement u is normalized into a nondimensional displacement $\tilde{u}$ using a characteristic length h as

$$\tau \equiv \frac{\omega t}{2\pi}, \quad \tilde{u} \equiv \frac{u}{h}, \tag{17a}$$

Eq. (16b) becomes

$$\frac{d^2\tilde{u}}{d\tau^2} + 2\zeta(2\pi)\frac{d\tilde{u}}{d\tau} + (2\pi)^2(\tilde{u} + \tilde{\alpha}\tilde{u}^3) = f_0 \sin \tilde{\Omega}\tau, \quad \tilde{\alpha} \equiv \alpha h^2, \ f_0 \equiv \frac{4\pi^2 F_0}{kh}, \quad \tilde{\Omega} \equiv \frac{2\pi\Omega}{\omega}. \tag{17b}$$

Note that Eq. (17b) is equivalent to Eq. (16b) with $\omega = 2\pi$ and $F = f_0$. Eq. (17b) has a linear natural frequency $\tilde{\omega} = 2\pi$ and a linear period $\tilde{T} = 1$ in the normalized time domain. After the answer $\tilde{u}$ is obtained in the τ domain, the actual answer can be obtained by scaling τ and $\tilde{u}$ back to the time t and the displacement u using Eq. (17a). In other words, the answer u obtained by solving Eq. (16b) with $\omega = 2\pi$ is valid for any value of ω if an appropriate scaling is used. Hence, without loss of generality we consider the nonlinear/nonstationary vibration of Eq. (16b) with:

$$\omega = 2\pi, \quad \zeta = 0.005, \quad \alpha = 1.7164,$$
$$u(0) = 1, \quad \dot{u}(0) = 0, \quad F = 5, \quad \Omega = 0.6\omega. \tag{18}$$

The α corresponds to the nonlinear first-mode vibration of a simply supported rectangular isotropic plate having four immovable edges, length : width : thickness =200:100:1, Young's modulus $E = 206\,\text{GPa}$,

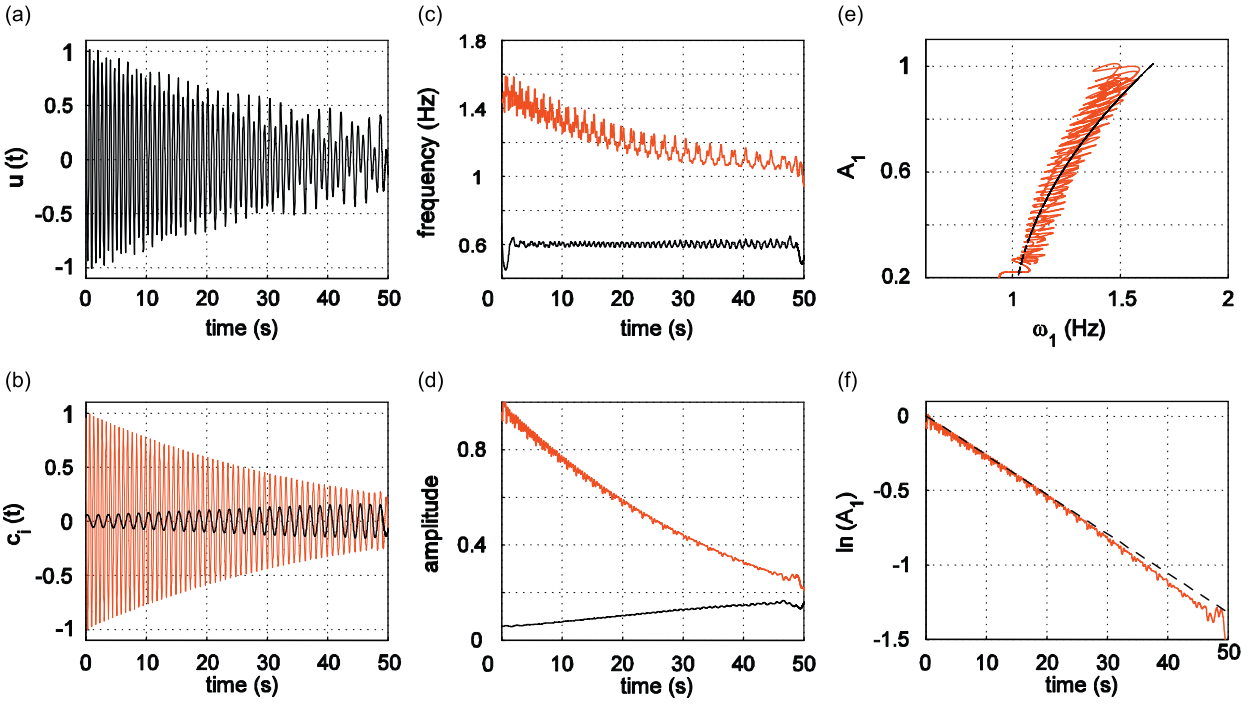

Fig. 1. HHT analysis of a nonlinear nonstationary response: (a) u, (b) c_1 (gray) and c_2 (black), (c) ω_1 (gray) and ω_2 (black), (d) A_1 (gray) and A_2 (black), (e) ω_1–A_1 curve (gray) and the backbone curve (black), and (f) $\ln(A_1(t))$.

Poisson's ratio $v = 0.3$, mass density $\rho = 7850\,\mathrm{kg/m^3}$, and the maximum displacement at the center being normalized with respect to the plate thickness [16]. Fig. 1 shows the results obtained from HHT analysis using a number of sampled points $N = 2^{12}$ and a sampling interval $\Delta t = 50.3/\mathrm{N}$. Fig. 1b shows that c_1 is the damped natural harmonic and c_2 is the distorted harmonic caused by the harmonic excitation with $\Omega = 0.6\,\mathrm{Hz}$ and the cubic nonlinearity. Fig. 1c and d shows that ω_1 modulates at $2\omega_1$ at the beginning, ω_2 modulates at $1.2\,\mathrm{Hz}\,(= 2\Omega)$, and ω_1 decreases with the amplitude A_1, indicating the existence of hardening cubic nonlinearity. Zoom-in views of Fig. 1d also show the existence of cubic nonlinearity because A_1 modulates at $2\omega_1$ when A_1 is large. If the $\omega_1(t)$ and $A_1(t)$ are curve-fitted using low-order polynomials, the $\omega_1 - A_1$ curve shown in Fig. 1e becomes a smooth averaged backbone curve (i.e., the middle line) bent to the right because of the hardening nonlinearity. However, because of high nonlinearity (i.e., large α), Fig. 1e shows that, as expected, the averaged backbone curve at large A_1 deviates from the backbone curve (broken line) from perturbation analysis with the assumption of weak nonlinearity. Because the damping is linear, the $\ln(A_1(t))$ in Fig. 1f should be a straight line if no nonlinearity exists. However, the nonlinear stiffness makes it slightly curved. More importantly, Fig. 1b and d shows that the amplitude A_2 is not constant and it gradually increases to approach its final steady-state value 0.185 when $t > 200$. This behavior is different from the prediction of the perturbation solution shown in Eq. (2b). This gradual increase of A_2 in Fig. 1d is caused by the nonlinearity and the coupling of transient and steady-state solutions, which is the reason why it often takes a long time for a nonlinear system to achieve a steady state.

If Eqs. (16b) and (18) with $F = 0$ is used, Fig. 2b shows that the time-varying A_1 remains almost the same as that in Fig. 1d, indicating that the transient part is not significantly affected by the forced response. Moreover, the zoom-in views shown in Fig. 2d clearly reveal that ω_1 and A_1 modulate at $2\omega_1$, indicating the influence of cubic nonlinearity. Furthermore, Fig. 2c shows that the middle line of the $\omega_1 - A_1$ curve agrees with the asymptotic backbone curve from perturbation analysis when A_1 is small.

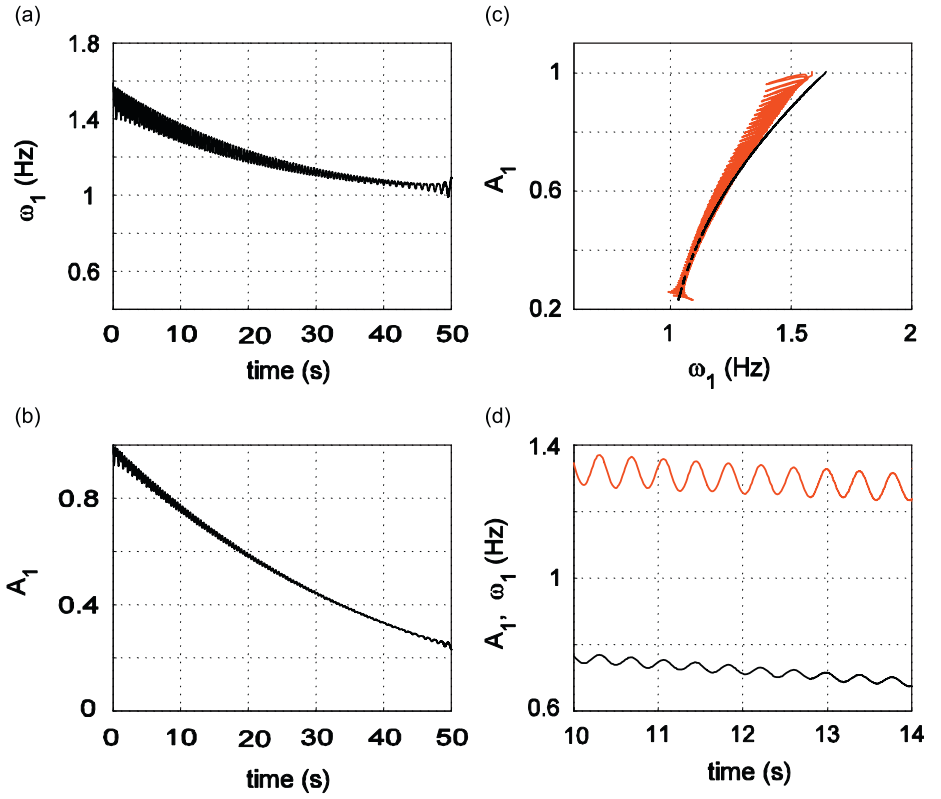

Fig. 2. HHT analysis of a nonlinear transient response: (a) $\omega_1(t)$, (b) $A_1(t)$, (c) ω_1–A_1 curve (gray) and the backbone curve (black), and (d) ω_1 (gray) and A_1 (black).

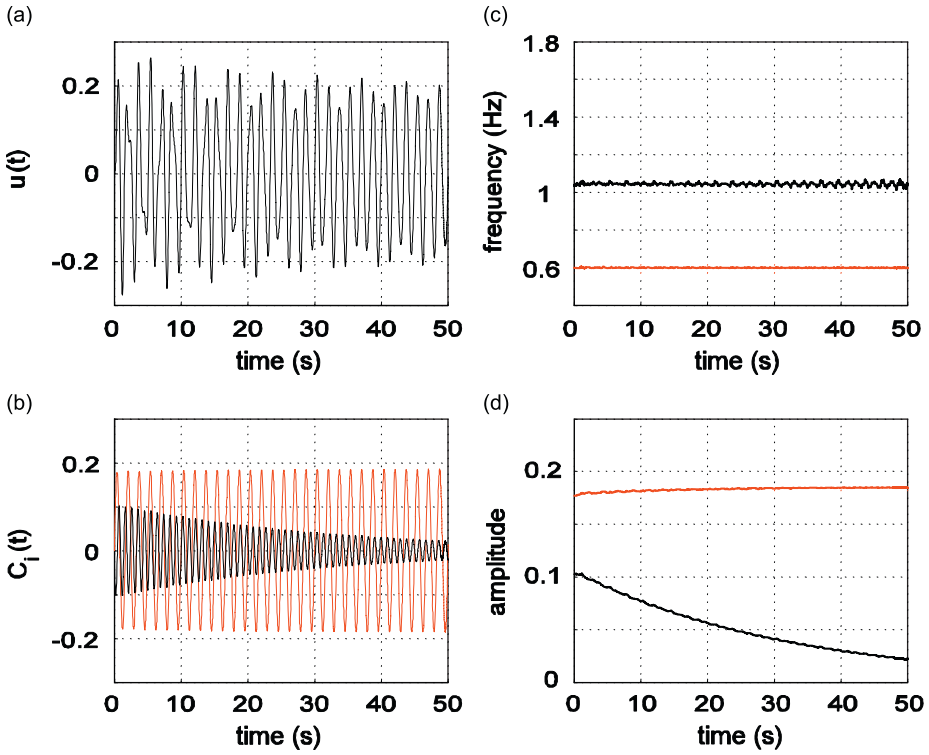

Fig. 3. SWF analysis of a nonlinear nonstationary response: (a) u, (b) C_1 (black) and C_2 (gray), (c) ω_1 (black) and ω_2 (gray), and (d) A_1 (black) and A_2 (gray).

If initial conditions are set to $u(0) = \dot{u}(0) = 0$ in Eqs. (16b) and (18), Fig. 3a–d shows the results from SWF analysis with the use of $\omega_1 = 1.04$ Hz and $\omega_2 = 0.6$ Hz in Eq. (3). The SWF cannot accurately extract the time-varying frequencies and amplitudes of the signals shown in Figs. 1 and 2 because the ω_1 varies from 1.5 to 1.0 Hz. However, because SWF is good at decomposing a signal consisting of regular harmonics and the ω_1 of this case does not vary significantly, the SWF is used here. Fig. 3b–d shows that the signal is decomposed into two distorted harmonics. More importantly, Fig. 3b and d shows that, at the beginning, the forced response C_2 has an amplitude close to but smaller than its final value 0.185, which reveals that the small start-up transient response C_1 still delays the development of the forced response but the influence is small. All these results indicate that the nonconstant forced response amplitude A_2 in Fig. 1d is indeed caused by the big transient response c_1.

For a linear system, the particular solution under a harmonic excitation should be a steady-state response with a constant amplitude starting from the beginning $t = 0$, as shown in Eq. (1a). If the nonlinear term is neglected by setting $\alpha = 0$ in Eqs. (16b) and (18), Fig. 4a–d shows the results from SWF analysis. With the use of $\omega_1 = 1$ Hz and $\omega_2 = 0.6$ Hz in Eq. (3), Fig. 4c and d shows that the signal is decomposed into two regular harmonics. More importantly, Fig. 4b and d shows that the steady-state component C_2 has a constant amplitude right from $t = 0$, which confirms the linear solution shown in Eq. (1a). Moreover, Figs. 4d, 1d, and 2b show that the transient part decays faster when there is no nonlinearity.

3.2. Two-degree-of-freedom system

We consider the following experimentally validated 2:1 vibration absorber for vibration suppression of the first-mode bending vibration u_2 of a cantilevered 42.0 cm × 6.35 cm × 1.28 mm stainless steel beam [3]

$$\ddot{u}_1 + \hat{\omega}_1^2 u_1 = g_{12} u_1 u_2, \tag{19a}$$

$$\ddot{u}_2 + 2\zeta_2\hat{\omega}_2\dot{u}_2 + \hat{\omega}_2^2 u_2 = g_{11}u_1^2 + F\cos\Omega t, \tag{19b}$$

$$\hat{\omega}_2 = 2\hat{\omega}_1 = 4\pi, \quad \zeta_2 = 0.0025, \quad u_1(0) = 0.03, \quad u_2(0) = 0.1, \quad \dot{u}_1(0) = \dot{u}_2(0) = 0, \quad g_{12} = 35.06, \quad g_{11} = 157.9,$$
$$F = 0.079, \quad \Omega = \hat{\omega}_2, \tag{19c}$$

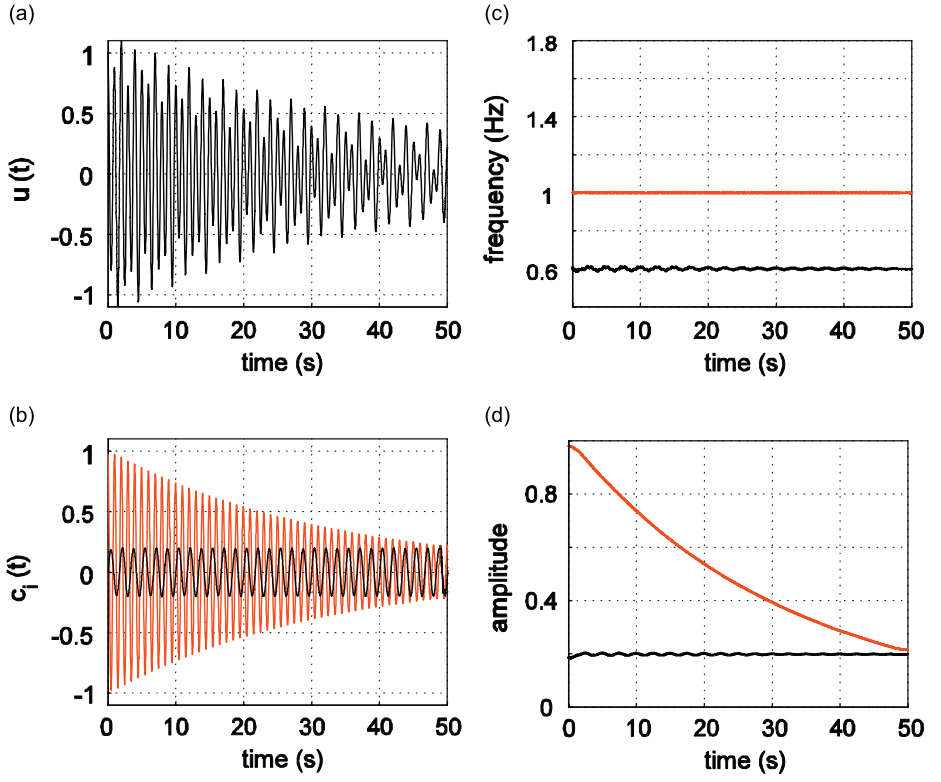

Fig. 4. SWF analysis of a linear nonstationary response: (a) u, (b) C_1 (gray) and C_2 (black), (c) ω_1 (gray) and ω_2 (black), and (d) A_1 (gray) and A_2 (black).

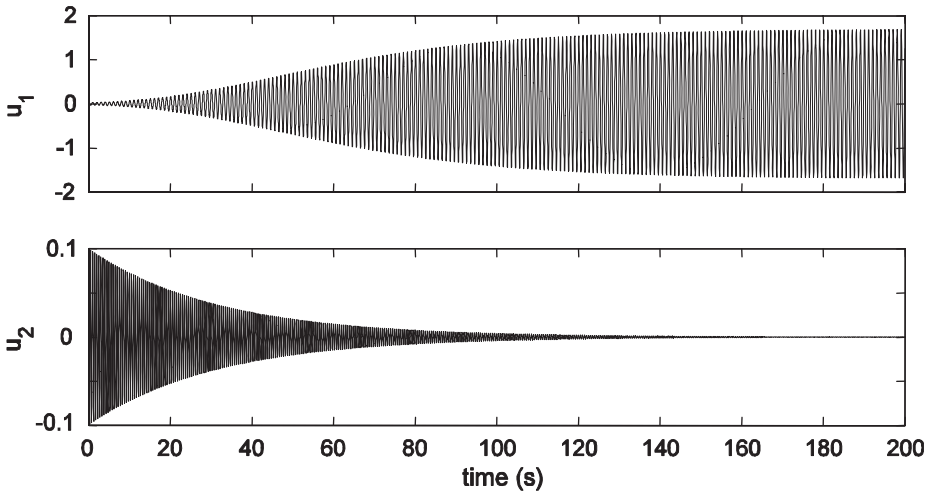

Fig. 5. The responses u_1 and u_2 of Eqs. (19a)–(19c) with $F = g_{11} = 0$.

where the time is normalized with respect to the linear undamped vibration period of the controller u_1, and $\Delta t = 0.02$ is used in the Runge–Kutta numerical integration. If Eqs. (19a)–(19c) with $F = g_{11} = 0$ are used, Fig. 5 shows that the linear free damped vibration u_2 has a frequency 2 Hz. Moreover, HHT analysis shows that the frequency of u_1 is 1 Hz with a small modulation at 2 Hz, which indicates that u_1 consists of 1 and 3 Hz harmonics (see Eq. (2c)). If Eqs. (19a)–(19c) with $F = 0$ are used, Fig. 6 shows that it takes much longer time for u_2 to die out because the nonlinear term $N_1(\equiv g_{11}u_1^2)$ couples u_2 and u_1 and hence the damping ζ_2 needs to damp out both u_2 and u_1. Again, HHT analysis shows that the frequency of u_1 is 1 Hz with a small modulation at 2 Hz, which indicates that u_1 consists of 1 and 3 Hz harmonics. Moreover, HHT analysis of u_2 shows that, when the amplitude is large, its frequency is about 1.995 Hz ($<\hat{\omega}_2 = 2$ Hz) because of the quadratic nonlinearity N_1 [1]. If Eqs. (19a)–(19c) with $g_{11} = 0$ are used, Fig. 7 shows that the linear forced response u_2 quickly grows to its steady amplitude 0.1 and the u_1 is forced by $N_2(\equiv g_{12}u_1u_2)$ at its linear resonant frequency $\hat{\omega}_1 = 1$ Hz.

If Eqs. (19a)–(19c) are used, Fig. 8 shows that the forced vibration u_2 is suppressed by $N_1(\equiv g_{11}u_1^2)$ to become a negligibly small constant and the u_1 has a small amplitude. Again, Fig. 9a from HHT analysis shows that the frequency of u_1 is 1 Hz with a small modulation at 2 Hz, which indicates that u_1 consists of 1 and 3 Hz harmonics. HHT analysis decomposes the nonlinear term $N_2(\equiv g_{12}u_1u_2)$ into $N_2 = c_{21} + c_{22}$. Fig. 9c and d

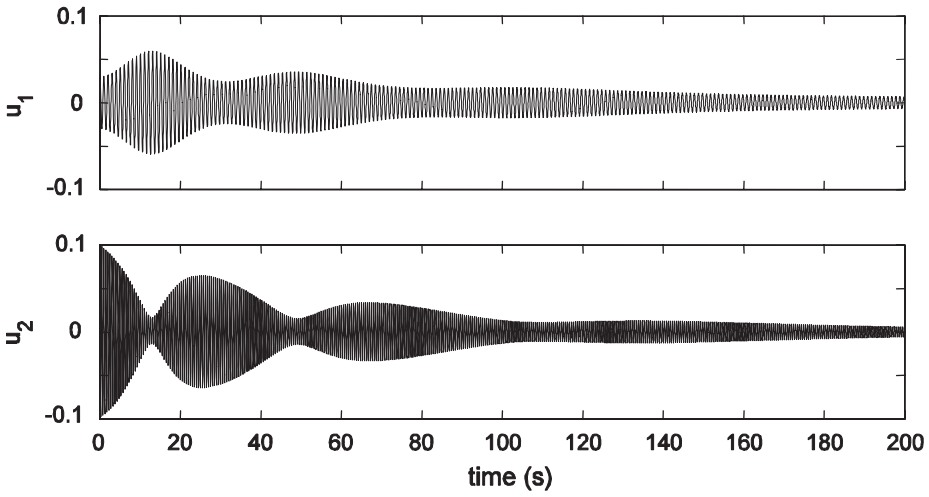

Fig. 6. The responses u_1 and u_2 of Eqs. (19a)–(19c) with $F = 0$.

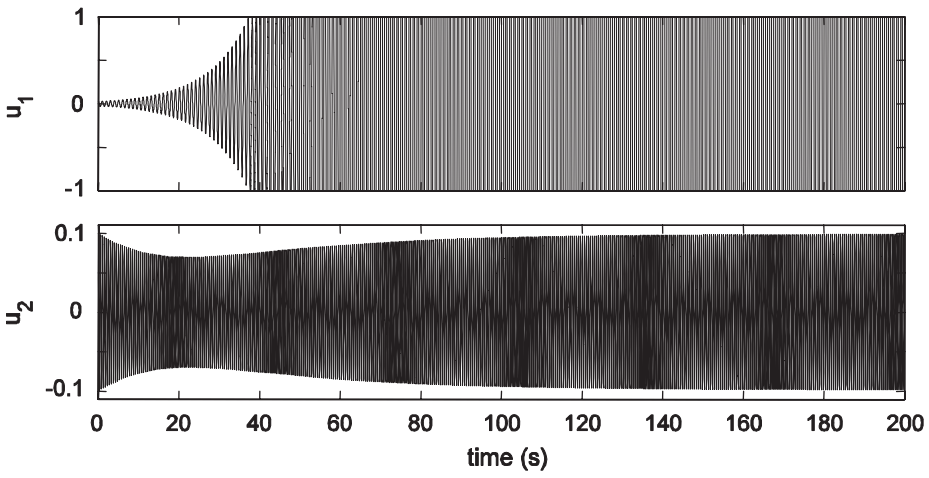

Fig. 7. The responses u_1 and u_2 of Eqs. (19a)–(19c) with $g_{11} = 0$.

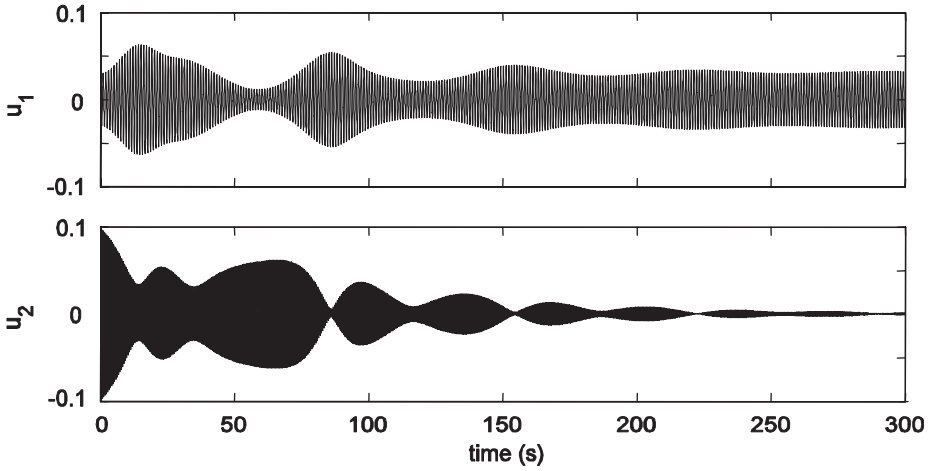

Fig. 8. The responses u_1 and u_2 of Eqs. (19a)–(19c).

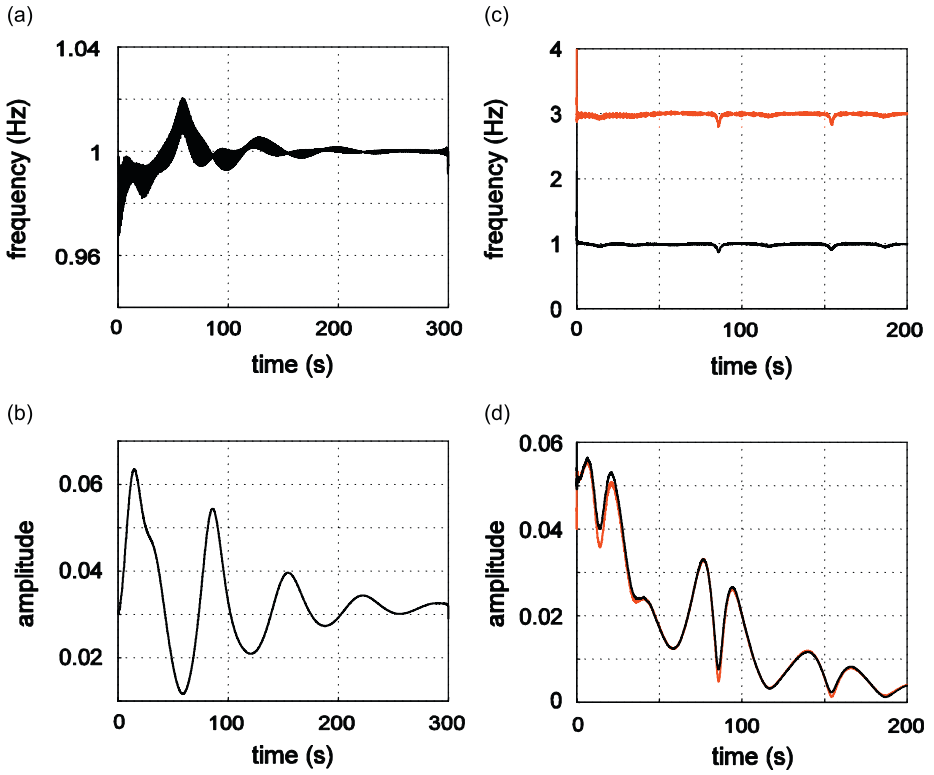

Fig. 9. HHT analysis: (a, b) the frequency ω_1 and amplitude A_1 of the u_1 in Fig. 8, and (c, d) ω_{21} (gray) and ω_{22} (black), and A_{21} (gray) and A_{22} (black) of N_2.

shows that c_{21} and c_{22} have almost the same amplitude but $\omega_{22} = \omega_{21}/3 = 1\,\text{Hz}$. Hence, the 1 Hz harmonic of u_1 is excited by c_{22} through resonance, and the small 3 Hz harmonic of u_1 is excited by c_{21} at a frequency away from resonance. This also reveals that the nonlinear term N_2 behaves like a cubic nonlinearity to u_1.

HHT analysis decomposes the nonlinear term N_1 ($\equiv g_{11}u_1^2$) into $N_1 = c_{11} + r_{11}$. Fig. 10c shows that ω_{11} is about 2 Hz and modulates at 2 Hz, indicating a quadratic nonlinearity. Moreover, Fig. 10d shows that the

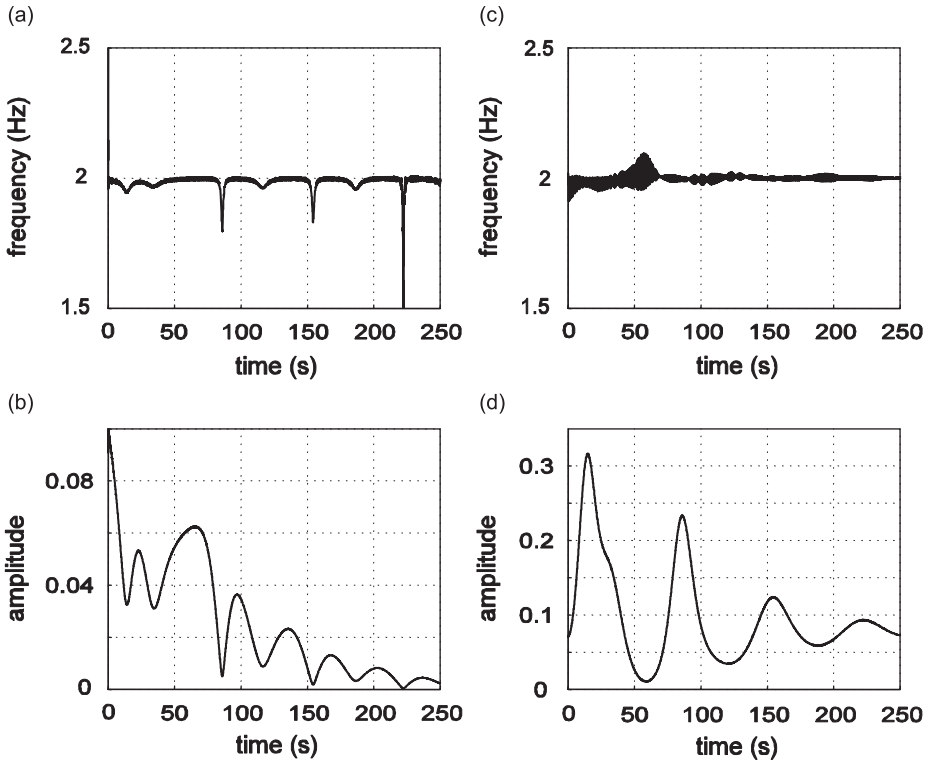

Fig. 10. HHT analysis: (a, b) the frequency ω_1 and amplitude A_1 of the u_2 in Fig. 8, and (c, d) ω_{11} and A_{11} $(=r_{11})$ of N_1.

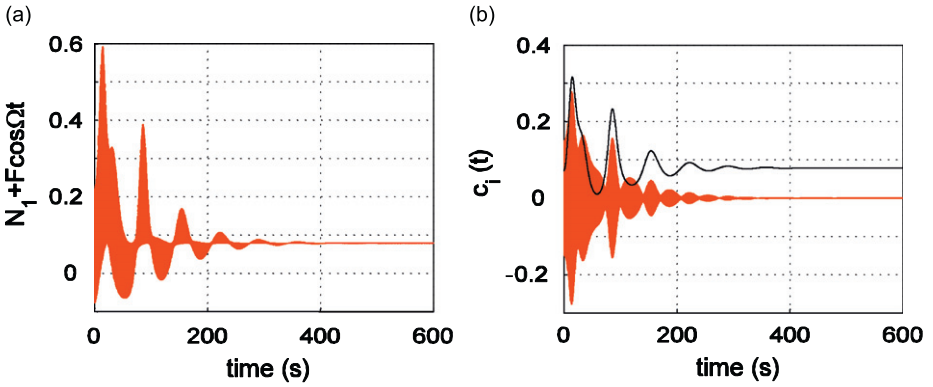

Fig. 11. HHT decomposition of $N_1 + F\cos\Omega t$ of Eqs. (19a)–(19c): (a) $N_1 + F\cos\Omega t$, and (b) c_1 (gray) and c_2 (black).

amplitude A_{11} is equal to the moving average r_{11} and their steady-state value is 0.079 ($= F$) after $t > 300$. In other words,

$$g_{11}u_1^2 = F + F\cos(\Omega t - \pi) = F - F\cos\Omega t. \tag{20}$$

Eq. (20) reveals that the nonlinear term N_1 results in a force to exactly balance out the external excitation force and force u_2 to have a negligibly small constant displacement $F/\hat{\omega}_2^2 = 0.0005$, which is confirmed by the zoom-in views of the u_2 at $t > 300$. This is the mechanism that makes this nonlinear vibration absorber work. Fig. 11 also confirms that $N_1 + F\cos\Omega t$ consists of one decaying harmonic and one moving average converging to a constant 0.079. Fig. 8 and Eq. (20) agree well with experimental results [3]. To explain the sudden change of ω_1 in Fig. 10a when $A_1 \approx 0$ let us consider a signal u consisting of two harmonics having two

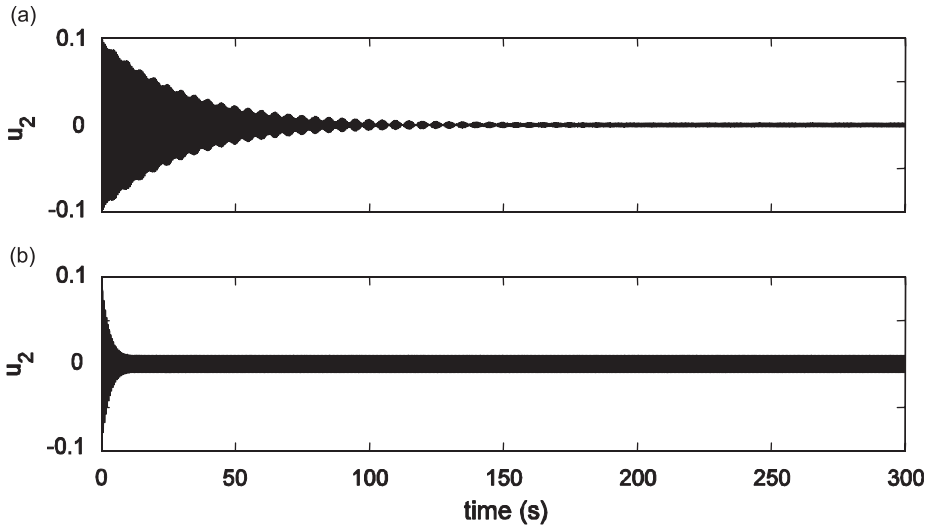

Fig. 12. The response u_2 of Eqs. (19b) and (19c) with $g_{11}=0$ and: (a) $\hat{\omega}_2=4.4\pi$, and (b) $\zeta_2=0.025$.

very close frequencies and amplitudes:

$$u=\frac{A}{2}\cos(\Omega+\varepsilon)t+\frac{A}{2}\cos(\Omega-\varepsilon)t=A\cos(\varepsilon t)\cos(\Omega t), \tag{21}$$

where ε is a small parameter. The amplitude $A\cos(\varepsilon t)$ changes sign, but amplitudes are assumed to be always positive during the EMD. Because of the nonpositive amplitude, the average of the upper and lower envelopes of u is nonzero (see Eq. (11)) and the extracted frequency becomes singular when $A\cos(\varepsilon t)=0$. Hence, the sudden change of ω_1 when $A_1\approx 0$ in Fig. 10a indicates that u_2 consists of two harmonics having two very close frequencies and amplitudes, which are caused by $F\cos\Omega t$ and N_1.

Fig. 12a shows that, if the natural frequency $\hat{\omega}_2$ (i.e., stiffness) is increased to 4.4π through a negative position feedback and Eqs. (19b) and (19c) with $g_{11}=0$ are used, the transient time is equivalent to that in Fig. 5 under linear free damped vibration. Fig. 12b shows that, if the damping ratio ζ_2 is increased to 0.025 through a negative velocity feedback and Eqs. (19b) and (19c) with $g_{11}=0$ are used, the transient time is smaller than that in Fig. 5 and much smaller than those in Figs. 6 and 8. Note that a position or velocity feedback controller works by changing the system parameters and its steady-state response is a harmonic with an amplitude A given by

$$A=\frac{F}{\bar{\omega}^2\sqrt{(1-\Omega^2/\bar{\omega}^2)^2+(2\bar{\zeta}\Omega/\bar{\omega})^2}}\neq\frac{F}{\hat{\omega}_2^2}, \tag{22}$$

where $\bar{\omega}$ and $\bar{\zeta}$ represent the $\hat{\omega}_2$ and ζ_2 modified by feedbacks. The amplitude A is often larger than $F/\hat{\omega}_2^2=0.0005$ because large feedbacks cause stability problems [3,4]. On the other hand, the nonlinear vibration absorber shown in Eqs. (19a) and (19b) works by using the nonlinear term N_1 ($\equiv g_{11}u_1^2$) to create a force to exactly balance out the external excitation force and force u_2 to have a negligibly small constant displacement $F/\hat{\omega}_2^2=0.0005$. Unfortunately, the nonlinear term results in a long transient time and limits the efficiency of this vibration absorber.

4. Concluding remarks

A method based on the empirical mode decomposition, Hilbert–Huang transform (HHT), and perturbation analysis is proposed for signal processing of nonlinear nonstationary vibration signals to investigate the long transient phenomenon in nonlinear structural vibrations. A sliding-window fitting (SWF) technique is also derived to show the physical implication of time–frequency signal decomposition. Because the HHT uses the

apparent time scales revealed by the signal's local maxima and minima to sequentially sift distorted harmonics of different time scales without using assumed basis functions and function orthogonality for component extraction, it provides time-varying amplitudes and frequencies of extracted distorted harmonics more accurate than those from the SWF analysis. On the other hand, because the SWF uses windowed regular harmonics and function orthogonality to simultaneously extract time-localized regular and/or distorted harmonics, it can provide accurate decomposition only for a signal consisting of regular harmonics. Based on numerical analyses of nonlinear systems of one and two degrees of freedom, it is concluded that the long transient phenomenon is caused by nonlinearities, coupling of transient and forced vibrations, and/or modal coupling of multiple modes.

References

[1] A.H. Nayfeh, D.T. Mook, *Nonlinear Oscillations*, Wiley-Interscience, New York, 1979.
[2] P.F. Pai, *Highly Flexible Structures: Modeling, Computation and Experimentation*, AIAA, Reston, Virginia, 2007.
[3] P.F. Pai, B. Wen, A.S. Naser, M.J. Schulz, Structural vibration control using PZT patches and nonlinear phenomena, *Journal of Sound and Vibration* 215 (1998) 273–296.
[4] P.F. Pai, B. Rommel, M.J. Schulz, Nonlinear vibration absorbers using higher-order internal resonances, *Journal of Sound and Vibration* 234 (2000) 799–817.
[5] D.J. Inman, *Engineering Vibration*, second ed., Prentice-Hall, New York, 2001.
[6] A.H. Nayfeh, *Introduction to Perturbation Techniques*, Wiley-Interscience, New York, 1981.
[7] N.E. Huang, Z. Shen, S.R. Long, M.C. Wu, H.H. Shih, Q. Zheng, N.C. Yen, C.C. Tung, H.H. Liu, The empirical mode decomposition and the Hilbert spectrum for nonlinear and non-stationary time series analysis, *Proceedings of the Royal Society of London Series A—Mathematical Physical and Engineering Sciences* 454 (1998) 903–995.
[8] N.E. Huang, Z. Shen, S.R. Long, A new view of nonlinear water waves: the Hilbert spectrum, *Annual Reviews of Fluid Mechanics* 31 (1999) 417–457.
[9] N.E. Huang, M.C. Wu, S.R. Long, S.S.P. Shen, W. Qu, P. Gloersen, K.L. Fan, A confidence limit for the empirical mode decomposition and Hilbert spectral analysis, *Proceedings of the Royal Society of London Series A—Mathematical Physical and Engineering Sciences* 459 (2003) 2317–2345.
[10] Q. Chen, N. Huang, S. Riemenschneider, Y. Xu, A B-spline approach for empirical mode decomposition, *Advances in Computational Mathematics* 24 (2006) 171–195.
[11] Z. Wu, N.E. Huang, A study of the characteristics of white noise using the empirical mode decomposition method, *Proceedings of the Royal Society of London Series A—Mathematical Physical and Engineering Sciences* 460 (2004) 1597–1611.
[12] N.E. Huang, N.O. Attoh-Okine (Eds.), *The Hilbert–Huang Transform in Engineering*, CRC Press, Boca Raton, FL, 2005.
[13] E.O. Brigham, *The Fast Fourier Transform*, Prentice-Hall, Englewood Cliffs, NJ, 1974.
[14] I. Daubechies, *Ten Lectures on Wavelets*, CBMS-NSF Lecture Notes, Vol. 61, SIAM, Philadelphia, 1992.
[15] G. Strang, T. Nguyen, *Wavelets and Filter Banks*, Wellesley-Cambridge Press, Wellesley, MA, 1997.
[16] B. Nageswara Rao, S.R.R. Pillai, Large-amplitude free vibrations of laminated anisotropic thin plates based on harmonic balance method, *Journal of Sound and Vibration* 154 (1992) 173–177.